Construction and Building Materials 363 (2023) 129803

Contents lists available at ScienceDirect

Construction and Building Materials

journal homepage: www.elsevier.com/locate/conbuildmat

Hardening characterisation of a non-proprietary and more eco-friendly UHPC

Ana Mafalda Matos [a,*], José Granja [b], Sandra Nunes [a,c], José L. Barroso-Aguiar [d], Miguel Azenha [b]

[a] CONSTRUCT-Labest, Faculty of Engineering (FEUP), University of Porto, Portugal
[b] ISISE, Department of Civil Engineering, University of Minho, Guimarães, Portugal
[c] Delft University of Technology (TU Delft), Delft, the Netherlands
[d] CTAC, Department of Civil Engineering, University of Minho, Guimarães, Portugal

ARTICLE INFO

Keywords:
Ultra-high performance fibre reinforced cementitious composites (UHPFRC)
Hardening
E-modulus
Autogenous shrinkage
Isothermal calorimetry

ABSTRACT

The current work provides an integrated analysis of autogenous shrinkage, isothermal calorimetry, and modulus of elasticity measurement through ambient response method (EMM-ARM), to characterise the hardening behaviour of a non-proprietary and more eco-friendly ultra-high performance fibre reinforced cementitious composite (UHPFRC). Isothermal calorimetry revealed that induction period ends at 3 h, and the rapid evolution of hydration heat occurs up to 9 h. Then, the hydration reaction still undergoes but at a very slow rate. The autogenous shrinkage exhibited a strong increase, particularly in the first 6 h, after which a dramatic reduction in the slope of the curves occurred, corroborating with the heat of hydration measurements. The modulus of elasticity evolution pattern revealed a typical cementitious material S-shaped curve, with a strong evolution in the first 8 h and reached 37 GPa at 7 days. As the current study perceives, UHPC/UHPFRC-3 % MOE evolution mainly occurs at very early ages. Thus, using EMM-ARM method for evaluating stiffness-related properties since casting age of UHPC/UHPFRC is of utmost importance to take advantage of the remarkable properties of such advanced material with no waste of time and resources. Furthermore, the UHPFRC developed with a lower amount of cement and silica fume decreases the heat of hydration, shrinkage, and reduced costs and ecological footprint without significantly impairing the MOE, compared to other non-proprietary blended UHPC/UHPFRC mixtures.

1. Introduction

It is well known that an adequate and functional infrastructure network is vital for developing a country or region and is directly related to economic and social prosperity. In Europe, most infrastructures are built in reinforced or prestressed concrete. Many of these structures are currently degraded due to exposure to aggressive environments and the significant load increase compared to the design phase. It is estimated that >50 % of the annual construction budget in Europe is spent on the rehabilitation, reinforcement or replacement of deteriorated concrete structures [1]. In addition to direct costs, the internalisation of costs associated with CO_2 emissions from construction and indirect costs for users due to restrictions on the use of infrastructure further increases the burden on society. Thus, construction stakeholders must provide more sustainable and resilient infrastructures, and it is of utmost importance the development new technologies rehabilitate existing structures and minimise maintenance interventions, ensuring a long and safe service life.

Abbreviations: CH, Calcium hydroxide; CO_2, Carbon dioxide; df, Diameter of fibres (mm); Dflow, Spread flow diameter (mm); EMM-ARM, E-Modulus Measurement through Ambient Response Method; LF, Limestone filler; lf, Length of fibres (mm); LVDT, Linear variable differential transformer; MOE, Modulus of Elasticity; $Q(t)$, Heat flow (kJ/kg); $\dot{Q}(t)$, Heat flow rate (W/kg); $\ddot{Q}(t)$, Energy acceleration (kJ/h^2); RH, Relative humidity (%); SCM, Supplementary cementitious materials; SEM, Scanning electron microscopy; SF, Silica fume; Sp, Polycarboxylate-based high-range water reducer; t, Time (days or hours); tf, Final setting time (h); t_{max}, Time of maximum heat flow rate (h); t_{min}, Time of minimum heat flow rate (h); REF, UHPC mixture including cement and limestone filler as binder; UHPFRC-3.0%, UHPFRC mixture including cement, limestone filler and silica fume as binder and 3.0% steel fibres (in volume); UHPC, Cementitious matrix of an UHPFRC; UHPFRC, Ultra-High Performance Fibre Reinforced Composite; UTT, Uniaxial tensile test; Vf, Volume of fibres (%); w/c, water to cement weight ratio; w/b, water to binder weight ratio; X, Fibre factor.

* Corresponding author.
E-mail address: ana.matos@fe.up.pt (A.M. Matos).

https://doi.org/10.1016/j.conbuildmat.2022.129803
Received 4 August 2022; Received in revised form 11 November 2022; Accepted 16 November 2022
Available online 16 December 2022

Ultra-high performance fibre reinforced composites (UHPFRC) are a new structural "concrete" generation. The main features are the remarkable mechanical performance, in which compressive and (uniaxial) tensile strength exceeds 130 MPa and 7 MPa, respectively (according to the French norm NF P 18–470), and excellent durability [2]. Those features are provided by the dense microstructure of the UHPC, with has almost no capillary pores and pore diameter between 0.1 and 0.001 μm, typically located within the C—S—H gel [3,2]. The fibres reinforcement (generally between 2 and 4 % by volume), surrounded by an ultra-compact cementitious matrix, provides high tensile strength, which may exhibit hardening behaviour and reasonable ductility. Besides, the possibility of self-compacting mixtures allows us to rethink the procedures for placing the UHPFRC. These mixtures can flow only under the action of their own weight, allowing, on the one hand, better distribution and orientation of the fibres and, on the other hand, facilitating the casting of slender elements and/or more complex shapes.

The raw materials selection and the mixture design are key steps for reaching UHPFRC performance. It is generally achieved by optimising the granular skeleton through a high amount of very fine powder materials, limiting the aggregate size to 1 mm and very low water content. The binder phase is usually a ternary blended, including i) a high proportion of cement (roughly 750 kg/m^3 [4]); ii) supplementary cementitious materials (SCM), which can be pozzolanic materials, such as silica fume (SF), fly ash (FA) or metakaolin (MTK), or latent hydraulic materials such as granulated blast furnace slag (GGBFS) (average amount of 200 kg/m^3 [4]); iii) nonreactive or very low reactive powders, such as quartz flour (QF) and limestone filler (LF) (average content 169 kg/m^3 [4]). The water/binder ratio (w/b) is very low, usually $<$0.20, which requires a high content of superplasticiser, usually PCE type (typically about 30 kg/m [4]). Besides, advanced curing regimes, such as heat treatment, steam curing, autoclave or pressure, are generally applied to speed up the hydration progression and increase microstructure density, thus contributing to outstanding mechanical performance even at early ages [4].

The cost of UHPFRC is one of the limitations in real construction projects because of the cost of some raw materials and eventual curing treatments. However, given its remarkable mechanical properties, it is estimated that the volume needed for UHPFRC is about 1/3 to 1/2 of the volume required of conventional concrete for comparable structural elements [5]. In addition, using UHPFRC may also not be necessary for the whole structure; sometimes, it is sufficient to use it in a selected area. Therefore, UHPFRC can be particularly exciting for rehabilitation projects due to its exceptional mechanical behaviour and durability properties, low porosity, micro-cracking control and self-compacting ability [6–8]. In this case, it might be a competitive technique since very small volumes of material are commonly needed (layers usually have 25–60 mm thickness). The concept consists of applying UHPFRC as a protective impermeable layer on elements or structures exposed to aggressive media and/or as a strengthening layer, which may include traditional reinforcement, on highly loaded areas. In this way, the structural capacity increases, durability significantly improves, and the initial cross-section is kept. Besides, the rapid development of mechanical properties reduces overall construction or intervention time. Indeed, over the last years, with the impulse of MCS/EPFL [9], among others [10], the application of cast "in situ" thin UHPFRC layers, for strengthening/rehabilitation of existing structures (buildings and bridges), has revealed several advantages in terms of durability, resilience, eco- and cost-efficiency, as well as small intervention duration with substantial benefits to the users [11,12,13,14,7,15,16,17,18,19]. Those features must be considered in an integrated life cycle cost analysis.

Even though autogenous shrinkage occurs in any concrete, this deformation is negligible in the case of ordinary vibrated concrete (such as a C25/30 concrete typically used in conventional construction). In the case of UHPFRC, this deformation is significant and particularly relevant to study in the case of rehabilitation applications [20–22]. The main cause of high autogenous shrinkage in UHPC/UHPFRC is its mixture composition, namely, low w/b ratio, high content of fine powder constituent materials, and no coarse aggregate. In fact, previous studies have shown that a significant portion of shrinkage occurs at a very early age, namely, up to 3 days of age [20,23,24]. Full-scale restrained shrinkage tests for thin UHPFRC slabs [25] revealed shrinkage cracks at a very early age (about 22 h and 19 h after casting). Besides, the high binder content usually provides high heat of hydration, which might cause shrinkage problems [26–29].

The evolution of the modulus of elasticity (MOE), shrinkage rate and level, tensile creep and strength have a key role in the magnitude of the internal stresses. Therefore, the very early age and evolution of strength and MOE of UHPFRC should be assessed, predicted and/or modelled to control or mitigate the possible premature shrinkage cracks in practical applications. MOE assessment by classic destructive approaches, such as standard cycling compression tests [30,31] has limitations. This testing method is time-consuming and does not allow the continuous monitoring of young modulus, and very early age assessment is not possible. In the last decades, several destructive and non-destructive test methods [32] have been under scrutiny by the scientific community to continuously measure the mechanical properties of cementitious materials from very early ages, namely:

1. Mechanical methods:
a) BTJASPE [33]
b) Temperature Stress Testing Machine [34,35].
2. wave propagation methods
a) wave transmission methods
   i. Ultrasound wave transmission [35]
   ii. bender-extender elements [35]
b) wave reflection methods [36]
3. Methods based on dielectric properties [36]
4. Classic resonance methods [37,38,39,32]

From the aforementioned methods, the most widely used for MOE determination are the resonant frequency-based methodologies and those based on ultra-sound wave propagation. Azenha et al. [40] proposed a variant of the classic resonant frequency methods for continuous evaluation of MOE evolution of cement-based materials, named E-Modulus Measurement through Ambient Response Method (EMM-ARM). The main feature of this methodology is the automatic and continuous assessment of MOE immediately after casting. In brief, a composite beam, including the material under study and a plastic mould, simply supported and with a certain geometry, is monitored with an accelerometer. The evolution of flexural resonant frequency of the first mode of vibration can be obtained by continuous non-parametric modal identification. Initially, the beam specimens (with concrete) were excited by the surrounding environmental noise (as people walking, wind, and noises from the construction site, among others). Those noises can conceptually be assumed as white noise, i.e., a stochastic process with constant spectral intensity in all frequencies [40]. Using the motion equation of a simply supported beam with a mass at mid-span, the stiffness evolution of the material can be computed based on the resonance frequency evolution of the composite beam. This method based has been successfully applied to concrete [32,40,41,42,43], cementitious pastes [32,44,45,46,47], confirming that EMM-ARM is able to measure with accuracy MOE in same testing conditions and ages, comparing with other conventional methods. The EMM-ARM methodology has continuously improved in the last years to be generally applied in both research and industry fields [48,49].

2. Research significance and objectives

UHPFRC may be an interesting advanced technology solution regarding sustainability, resilience and ecological footprint. However, its use in practice is still rare because of economically competitive solutions, particularly in Portugal. UHPFRC patented blended mixtures

commercially available in Europe have limited price competitiveness, a limited number of suppliers and a lack of control over the raw materials. Some research groups have been studying alternative UHPFRC mixtures and using local and more eco- and cost-effective constituent raw materials, including agricultural or industrial by-products/waste materials [50–55], coarse aggregates [56–58], aiming to reduce both cost and carbon footprint of producing UHPFRC. Accordingly, in CONSTRUCT-FEUP, research projects have been carried out to develop robust and more eco- and cost-efficient UHPFRCs employing locally available raw materials and conventional curing methods, scaled to the performance requirements, to demonstrate the applicability and advantages of this material namely in repair/rehabilitation applications [2,59–64].

Particulary for rehabilitation/strengthening applications, the stresses created by autogenous shrinkage can be higher or lower depending on the relevance of the MOE along the shrinkage development process. Thus, it is essential to improve understanding of the original kinetics observed on autogenous shrinkage of the new UHPFRC and describe the early age MOE evolution. From the literature survey, MOE results of UHPC/UHPFRC, both commercially available or non-property mixtures, revealed that most of the studies rely on classic cyclic load tests following the standardized tests [65,28] as ASTM C469 [65–69], DIN EN 12390, BS 1881–121 [70,71], *ACI* 318–11 [72], and most of them were performed at 28 days (see Appendix A). At that age, the MOE ranges between 37 and 58 GPa, depending on several factors such as curing treatment applied, w/c ratio, type of aggregate employed, and type of SCM (see Appendix A). Even though there is already literature on non-destructive test methods applied to UHPC to estimate mechanical properties [73,71], such as compressive strength and MOE, the continuous characterisation of the evolution of MOE since very early ages is lacking. Previous studies [74] have reported that this type of cement-based material's MOE increases with time, but the increase is small after three days. As best to the author's knowledge, only Yoo et al. [56] assessed early tensile MOE of UHPC, since casting, by UPV. Other early age measurements found correspond to 1 old day [73] using UPV measurements by commercially available equipment (direct transmission), Rebound hammer (RH) and Sonreb (combination of UPV and RH).

For the first time the current work provides UHPC/UHPFRC MOE assessment since casting using the innovative, real-time and non-destructive method, the EMM-ARM. Besides, an integrated analysis with different methodologies, including, setting time, autogenous shrinkage and isothermal calorimetry was was performed. Major objective of this research was compare aging characteristics obtained among different methodologies and check simultaneity of MOE evolution inflections with autogenous shrinkage behaviour and hydration kinectis.

3. Materials and methods

3.1. Raw materials and mixture design

The mixture design of UHPFRC has some apparent disadvantages in terms of cost, limited availability and carbon footprint due to the high need for PC and SF. Besides, UHPFRC applications rely mostly on the prefabrication industry, as such special production and curing methods are generally employed, and therefore extra financial and environmental costs. These restrictions motivated designing and optimising mixtures using locally available raw materials and lower amounts of cement and SF. The UHPFRC under study was particularly developed for rehabilitation/strengthening of concrete structures, requiring on-site casting, and common technology, such as conventional curing, while keeping ultra-high strength [59].

The new UHPFRC formulation developed by the authors incorporated the following constituent locally available raw materials (detailed information can be found in [63]): Portland cement CEM I 42.5R (EN 197–1), containing at least 95 % of clinker, which the principal constituents of main clinker phases, given by Bogue's formula, are: C_3S = 55.65 %, C_2S = 14.86, C_3A 8.12 % and C_4AF = 9.62 %; dry micro silica fume powder (SF); limestone filler (LF); the aggregate fraction is composed by 15 % of ECat, which is a waste material generated by Portuguese refinery company (density 2660 kg/m^3, water absorption 30 %) and 75 % of natural siliceous sand with a maximum particle size of 1 mm (density 2570 kg/m^3 and water absorption 0.5 %); polycarboxylate type high water reducer; potable water (according to standard EN 1008). The fibre reinforced composite, UHPFRC-3 %, incorporated 3 % by volume of micro steel fibres with 13 mm in length and 0.2 mm in diameter, with tensile strength of 2750 MPa and modulus of elasticity of 200 GPa. Table 1 summarises the main oxide composition, pozzolanicity, and physical and mechanical properties of cement, SF, LF and ECat.

Table 1
Main oxide composition, LOI and physical properties of cement, silica fume, limestone filler and ECat.

		CEM I 42.5 R	*Silica Fume*	*Limestone filler*	*ECat*
Main oxide composition and LOI (%)	LOI	2.67	<3		1.05
	Insoluble residue	1.00			
	SiO_2	19.38	>90		40.30
	Al_2O_3	5.12			54.45
	Fe_2O_3	3.28		0.02	0.45
	CaO	62.25		99.00	0.06
	MgO	1.57		0.30	0.15
	Na_2O	0.13			0.43
	K_2O	0.55			0.02
	SO_3	3.22		<0.05	0.00
	Cl	0.05		<0.001	
	Free lime	1.28			
Pozzolanic reactivity (NF P18-513)	mg Ca $(OH)_2$/ g		1577		1540
Physical properties	Density (kg/m^3)	3110	2200	2680	2660
	Specific surface (kg/ m^2)	439.5 (Blaine)	19 632 (BET)	540 (Blaine)	150 000 (BET)
Mechanical properties	Rc,2	32.2			
	Rc,7	47.4			
	Rc,28	60.8			

Fig. 1 depicts the morphology of the cement, LF, silica fume, ECat particles, and steel fibres observed by SEM Secondary Electrons mode. Cement particles are irregular and present a wide range of sizes, while ECat particles are rounded with rough surface texture and narrow size distribution. Silica fume particles are very spherical with nano-scale dimensions.

The Design of Experiments (combining statistical methods, regression analysis and optimisation techniques) allowed achieving the various performance requirements of the new UHPC, namely, self-compacting ability, low autogenous shrinkage, high durability and compressive strength 130 MPa without heat treatments or other accelerated curing processes. The incorporation of ECat, a local industrial waste, reduced the mixture's cost and ecological footprint, acting as internal curing agent due to high water absorption capacity and thus mitigating autogenous shrinkage [59,63].

The optimum compositions of the new composite with fibres (UHPFRC-3 %) and without fibres (UHPC) are presented in Table 2. A reference mixture (REF mixture in Table 2), including cement and limestone filler as a binder, was used in the current study for comparison purposes.

The optimal UHPC mixture was reinforced with 3 % (by volume) high-strength micro steel fibres (UHPFRC-3 %) and presented similar performance compared to commercially blended mixtures with higher cement and silica fume dosages and also compared with other non-property mixtures. The compressive strength between 2 and 90 days is

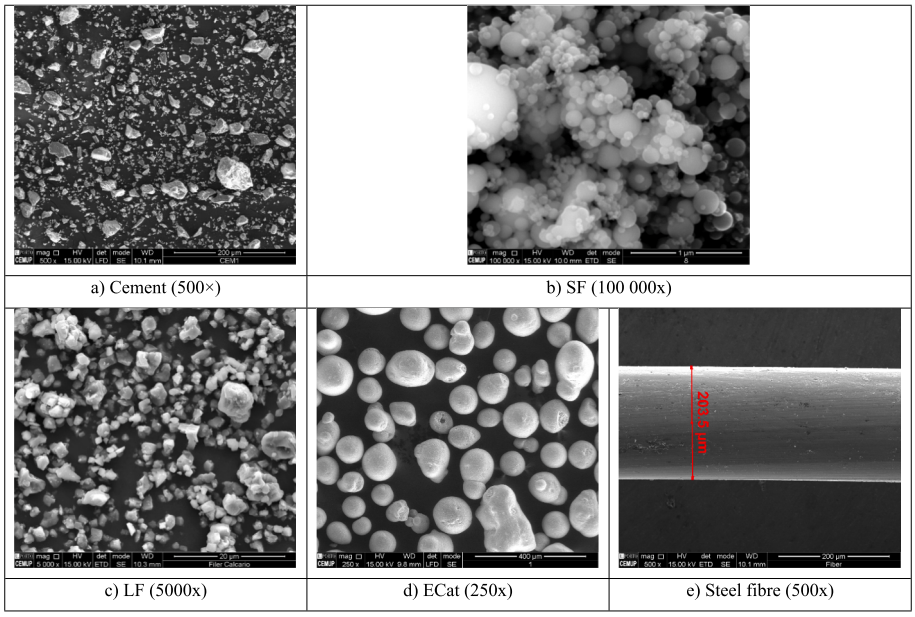

Fig. 1. Secondary electron mode SEM image of: a) cement particles; b) Silica fume particles; c) Limestont filler particles; d) Ecat particles; e) a micro Steel fibre.

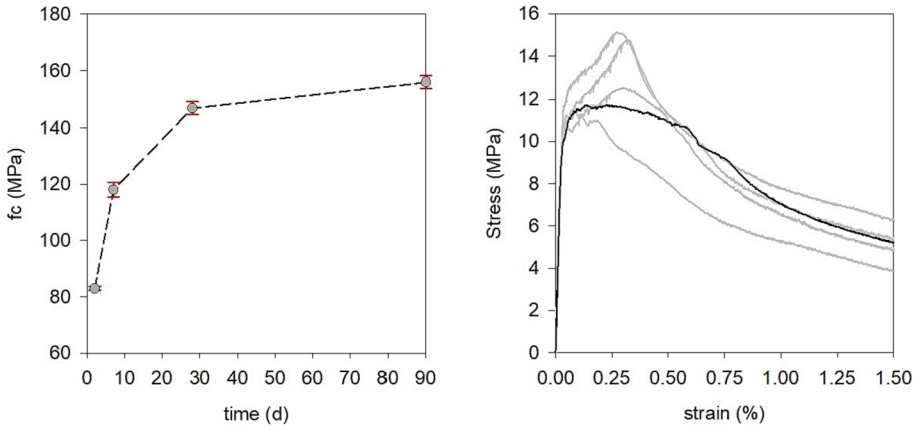

Fig. 2. a) compressive strength evolution of UHPFRC-3 % (cubes 50 mm); b) Uniaxial tensile behaviour at 28 days in dog bone specimens ([63]).

presented in Fig. 2-a and 147 and 156 MPa were reached after 28 and 90 days in UHPFRC-3 % conventional water cured specimens, respectively. At 2 days, UHPFRC-3 % specimens reached 53 % of the compressive strength at 90 days. This was followed by a less pronounced rate of compressive strength development in the subsequent days, being, respectively, at 7 days and 28 days, 76 % and 94 % of the ultimate compressive strength at 90 days.

Table 2
Mixture design of REF, UHPC and UHPFRC-3%.

Raw materials		REF (kg/m3)	UHPC (kg/m3)	UHPFRC-3% (kg/m3)
Binder	Cement	885.91	690.19	690.19
	Silica fume	–	33.56	33.56
	Limestone	311.43	250.58	250.58
Aggregates	ECat	–	155.45	155.45
	Sand	1019.86	852.11	775.01
Admixture and water	Superplasticizer	22.00	19.49	19.49
	Potable Water	182.50	160.86	160.86
Reinforcement	Short steel fibres	–	–	235.00

Fig. 2-b presents the uniaxial tensile behaviour of UHPFRC-3 % and peak stress from 11 to 15 MPa and peak strain ranging from 0.27 to 0.47 % were obtained at 28 days [63,75] in water-cured specimens. The individual specimens stress–strain curves are presented in grey colour in Fig. 2-b, as well as the average curve in black colour. A significant tensile-hardening branch was observed in most specimens, particularly, for the specimens with more favourable fibres orientation. In all of the individual curves, three main stages can be identified: elastic, hardening and softening. In the first stage, a linear elastic behaviour is observed until the first single micro-crack forms. After matrix cracking, an increase in stress was always observed, which is accompanied by the formation of multiple micro-cracks. The last stage starts when a macro-crack localises in one of the previously formed micro-cracks, being characterised by a decrease in stress. The testing details can be found in previous work [55].

Besides, the new eco-friendly UHPC standard durability indicators proved to be similar to other UHPFRC/UHPC non-proprietary or commercially blended mixtures [2,76]. The durability study in cracked UHPFRC specimens outcome that even cracked new UHPFRC can act as a protective layer against aggressive aqueous media, and a cover layer of at least 20 mm would be recommended when exposed to chloride environment (XS3/XS4) [61,60].

Table 3
Experimental tests summary.

Property	*Test standard or procedure*	*Testing age*	*Number of specimens*	*Samples geometry*
Slum flow diameter	EFNARC Section 3.2.1	After mixing	Each batch	–
Final setting time	EN 196–3 Section 3.2.1	After mixing	3	Vicat mould
Heat generation	Section 3.2.2	After mixing up to 3 days	6	–
Autogenous shrinkage	ASTM C1698 Section 3.2.3	After final setting time to 7 days	3	corrugated moulds specimens (length 440 mm and average diameter 28.5 mm)
Young Modulus	EMM-ARM Section 3.2.4	After mixing up to 7 days	6	tube moulds with 550 mm length and external/internal diameters of 50/44 mm

3.2. UHPC/UHPFRC early age characterisation

The mixtures presented in Table 2 were prepared using a mortar mixer in accordance with EN 196-1, and the operation speed adopted during all procedure was 140 ± 5 rotations·min^{-1}. The mixing sequence was: i) Mixing ECat with water-1 during 5 min; ii) Adding cement + limestone filler + silica fume + sand and mixing for 2.5 min; iii) Adding water-2 plus 75 % of Sp and mixing for 2.5 min; iv) Adding the remaining Sp and mixing for 1.5 min; v) Adding fibres and mixing during 2 min (for UHPFRC-3 % only). Water-1 corresponds to 80 % of the mixing water indicated in Table 2 plus the absorption water of ECat; and Water-2 corresponds to 20 % of the mixing water indicated in Table 2.

The fresh and hardening of REF, UHPC and UHPFRC-3.0 % mixtures were assessed through flow diameter (section 3.2.1), final setting time (section 3.2.1), isothermal calorimetry on equivalent pastes mixtures (section 3.2.2), autogenous shrinkage (section 3.2.3) and young modulus since casting using EMM-ARM methodology (section 3.2.4). Table 3 presents the experimental programme summary, and the following sections describe the testing methods in more detail.

3.2.1. Flowability and final setting time

The flowability capacity of the mixtures was assessed immediately after mixing through the mini-slump flow test following the EFNARC recommendations. A mini-cone was filled with a sample of fresh material. After removing the mini-cone, the material flowed until reaching a steady, stable state corresponding to a pancake-like shape. The test result is the spread flow diameter corresponding to the average value of two measurements made in two perpendicular directions (Dflow). The EN 196–1 procedure was followed to measure the final setting time of mixtures under study, under a controlled environment room (T = 20 ± 2 °C and HR = 50 ± 5 %), using Vicat apparatus.

3.2.2. Characterising heat generation

The characterisation of heat generation was performed on a JAF60 isothermal calorimeter [77]. The equipment consists of a calorimetric unit kept inside a constant temperature bath (see Fig. 3). Immediately after mixing, the pastes samples were poured inside a plastic bag and sealed. All paste samples studied contained 30 g of cement.

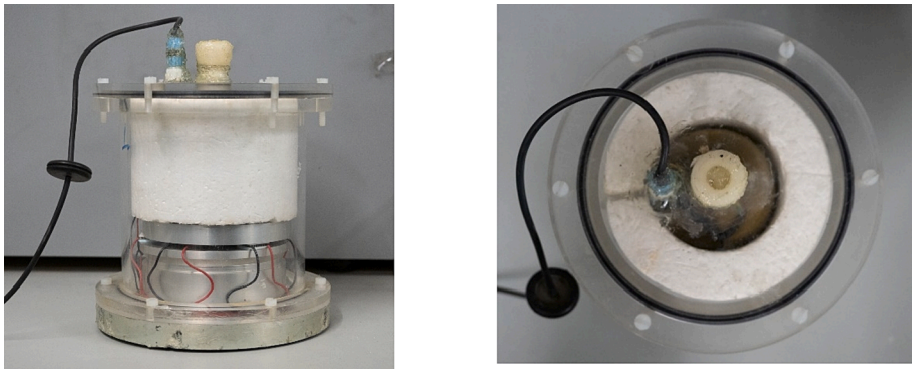

Fig. 3. Calorimetric unit of JAF60 isothermal calorimeter.

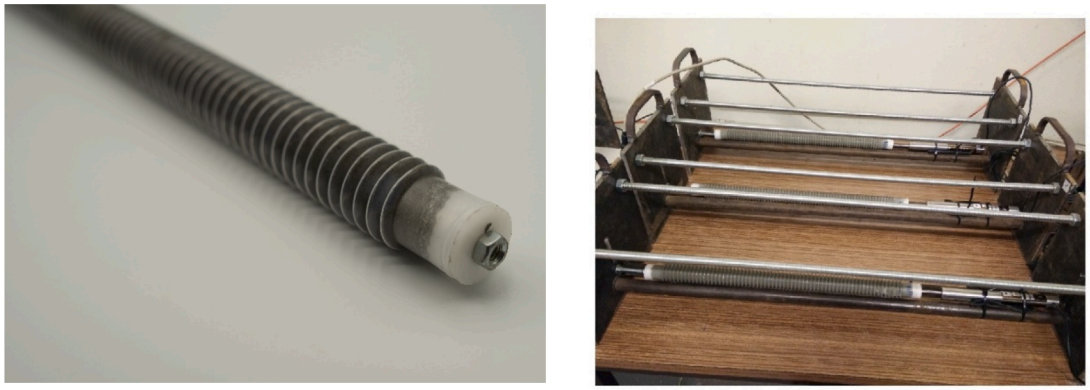

a) b)

Fig. 4. a) Corrugated moulds for autogenous shrinkage measurement: b) Autogenous shrinkage set-up.

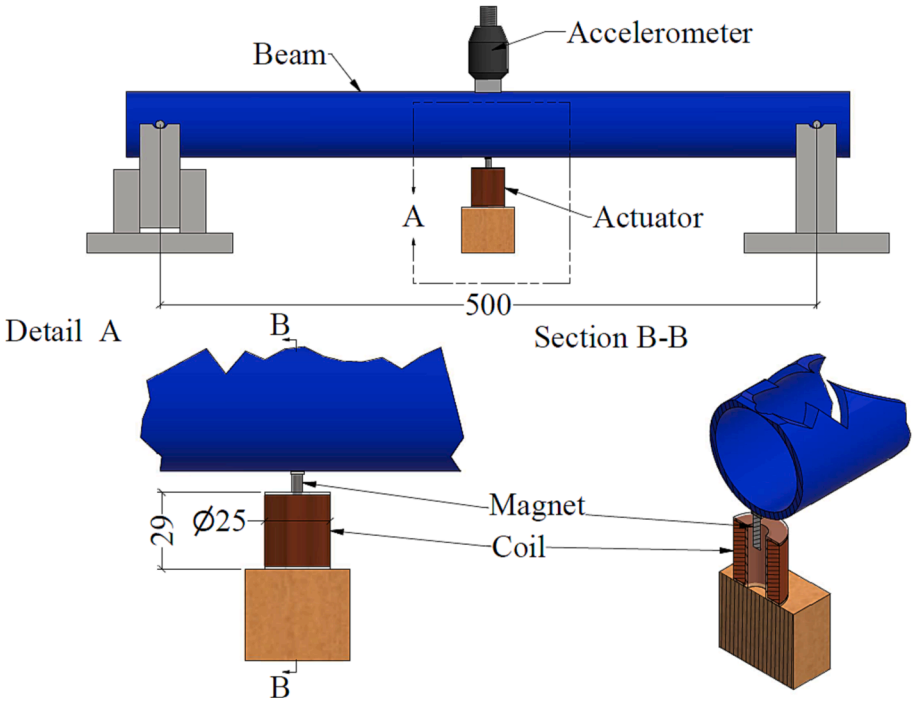

Fig. 5. Schematic view of custom-made non-contact electromagnetic actuator attached to an EMM-ARM beam (units: mm), adapted from [49].

a) b)

Fig. 6. EMM-ARM beam: a) accelerometer at mid-span; b) full view.

Measurements started 30 min after 't = 0′ (water addition to powder materials) and lasted 3 days.

The plastic bag containing the fresh paste was placed inside a brass container in the lower part of the unit, in direct contact with a heat sink. At the same time, the remaining surfaces were thermally insulated from the effects of the surrounding bath through a polystyrene envelope, see Fig. 3. The generated heat from the exothermic cement hydration reaction was conducted in a constant temperature bath (in this study 20 °C) through the heat sink. Between the paste sample container and the heat sink, the heat flux sensors generate an output voltage proportional to the heat flow of heat, which allows measuring the heat generated from the sample hydration reaction. Six samples were tested for each sample paste, REF and UHPC.

3.2.3. *Autogenous shrinkage deformation*

ASTM C1698 procedure was followed to assess the linear autogenous shrinkage deformation of mixture compositions presented in Table 2. In brief, three sealed corrugated moulds specimens (with a length of 440 mm and an average diameter of 28.5 mm, see Fig. 4-a) were cast for each mix composition. Afterwards, each specimen was weighted and kept in a controlled environment room (T = 20 ± 2 °C and RH = 50 ± 5 %). The final setting time, determined according to the procedure described in Section 3.2.1, was considered "time-zero" for assessing linear autogenous shrinkage length change. At that time, the length of each tube specimen was measured, which was considered the specimen's initial length. The current study recorded linear shrinkage deformations continuously (every minute) employing DC LVDT with an accuracy of 0.001 mm and a dataTaker DT500 acquisition system up to 7 days (168 h), as depicted in Fig. 4-b. The autogenous shrinkage results are the average of three samples for each mixture, REF, UHPC and UHPFRC-3 %.

3.2.4. *EMM-ARM*

The EMM-ARM was performed using PVC tube moulds 550 mm long and external/internal diameters 50/44 mm. This configuration, shown in the scheme of Fig. 5 and the photos of Fig. 6, allows the structure to act as a 500 mm free-span simply supported beam. A custom electromagnetic actuator, developed by Granja [48], was positioned at the mid-span of the beam specimen, applying, without contact, a sinusoidal force with linear variation in frequency (between 20 and 200 Hz) for 40 s. The

Table 4
Flowability and final setting time for REF, UHPC and UHPFRC-3%.

	Dflow (mm)	tf (hh:mm)
REF	280	02:45
UHPC	312	02:30
UHPFRC-3 %	283	02:00

signal sent to the actuator had an amplitude of ± 2.4 V and was sent through a dynamic signal analyser NI 4431 with a 24-bit resolution at a sampling frequency of 20 kHz. The induced accelerations were measured using a piezoelectric accelerometer (PCB 288D01 with a sensitivity to accelerations of 100 mV/g in the range of reading ± 50 g and sensitivity to forces of 22.4 mV/N in the field of reading ± 222.4 N) [49]. The testing details can be found in [49].

After mixing, the mixtures were deposited in the EMM-ARM test moulds with an inclination of 45°. While casting, the PVC moulds were vibrated to expel air bubbles before closing the mould. Then, each tube was placed horizontally at the final testing position, and the accelerometer was screwed to the mid-span. Vertical accelerations measurement started approximately 30 min after 't = 0′, and were performed continuously for a minimum period of 7 days in a controlled environment (T = 20 ± 2 °C). At least 6 samples were tested for each mixture presented in Table 2 (REF, UHPC and UHPFRC-3 %), and the EMM-ARM results correspond to the average value for each mixture.

4. Results and discussion

4.1. Flowability and setting time

The ease of casting with UHPFRC is a major concern due to extremely low water content (as discussed in section 1), which might reduce workability. Generally, UHPFRC is self-compacting in the fresh state. Some studies recommended a flow diameter spread between 200 and 350 mm according to ASTM C230 for UHPFRC without fibres [19,78]. Other researchers suggest a slump flow of 280 ± 10 mm to ensure low air entrapment and good flowability [79].

The UHPC/UHPFRC-3 % took advantage of the well-known positive effect of limestone fillers on workability helping in cement/superplasticisers compatibility issues [80,81]. In addition, the silica fume used presents extremely small spherical particles (see Fig. 1-b), improving the workability due to the increased packing density [48]. This can be seen comparing the REF and UHPC mixtures spread flow diameter, shown in Table 4. REF and UHPC present similar Sp/p and w/c (see Table 2), however, the spread flow diameter was significantly higher in UHPC mixture, 312 mm, while in REF was 280 mm.

As expected, adding steel fibres, decreases the flowability [82,83]. The fibre factor (χ) accounts the mutual effect of fibre content and fibres aspect ratio [84]. A fibre factor below 2 is usually recommended to preserve the workability of UHPFRC without fibre clumping [85]. In the present study, the fibre factor was 1.80. No significant loss of workability occurred, and cast mixtures satisfied the desired flowability of fresh UHPFRC. Besides, no segregation was observed.

Table 4 summarises the obtained results of the final setting time for all studied mixtures. A wider range of UHPC setting times can be found in the literature survey [86,87]. This is mainly because it varies significantly with the type and amount of superplasticiser, cement and SCM employed. However, it can be noted that final setting times decrease with SF increase content (from 0 % to 5 % cement replacement, mixture REF and UHPC, respectively). The addition of fine SF particles provides larger surface area that facilitates the nucleation and precipitation of hydration products, thus bolstering the growth of hydrates and increasing their connectivity within the microstructure. This manifests as shorter times of initial and final setting [76]. Besides, previous research studies also showed ECat decreases the setting time [63,88,89,90], due to its high reactivity, similar to that of silica fume (see Table 1) and high water absorption capacity (30 % by mass, as detailed in section 3.1).

Table 5
Hydration characteristics of UHPC mixture.

UHPC pastes	End of induction period		Peak of hydration		Cumulative heat	
	$\dot{Q}$ min (W/kg)	$t_{\dot{Q}min}$(h)	$t_{\dot{Q}max}$(h)	$\dot{Q}$ max (W/kg cement)	Q– 24 h (kJ/kg)	Q- 72 h (kJ/kg)
Sample 1	0.40	3.20	8.50	2.88	121.12	176.92
Sample 2	0.40	3.20	8.40	2.89	130.45	183.16
Sample 3	0.50	2.80	8.70	3.15	131.79	189.94
Sample 4	0.50	2.80	8.70	3.02	128.64	187.57
Sample 5	0.48	2.40	8.00	2.96	126.51	181.24
Sample 6	0.44	2.70	8.80	3.00	126.35	176.72
Average	0.45	2.85	8.52	2.98	127.48	182.59
Std. Dev.	0.05	0.31	0.29	0.10	3.78	5.43

4.2. Hydration kinetics

Fig. 7-b presents the individual cumulative heat curves for REF (six grey lines corresponding to 6 repetitions of the experiment with equally prepared specimens) and UHPC mixtures (6 black lines corresponding to

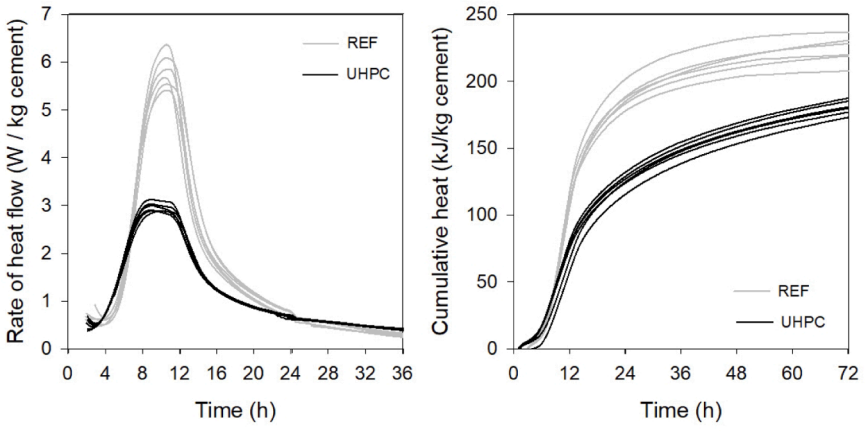

Fig. 7. a) Heat of hydration development and b) cumulative heat for REF and UHPC paste samples.

Table 6
Hydration characteristics of REF mixture.

REF pastes	End of induction period		Peak of hydration		Cumulative heat	
	$\dot{Q}$ min (W/kg)	$t_{\dot{Q}min}$(h)	$t_{\dot{Q}max}$(h)	$\dot{Q}$ max (W/kg cement)	$Q-$ 24 h (kJ/kg)	Q- 72 h (kJ/kg)
Sample 1	0.61	3.80	10.20	6.10	202.43	237.25
Sample 2	0.51	3.70	10.00	5.59	189.16	229.05
Sample 3	0.64	4.00	10.60	6.39	188.11	219.98
Sample 4	0.64	4.00	10.00	5.90	183.87	219.26
Sample 5	0.49	3.00	10.50	5.71	178.51	208.11
Sample 6	0.61	3.10	10.80	5.46	185.77	232.23
Average	0.58	3.60	10.35	5.86	187.97	224.31
Std. Dev.	0.07	0.44	0.33	0.34	8.02	10.58

6 repetitions of the experiment with equally prepared specimens). In addition, the individual reaction heat flow curves are depicted in Fig. 7-a, for REF (grey lines) and UHPC mixtures (black lines). Moreover, Table 5 and Table 6 summarise the main measured characteristics values based on isothermal hydration curves, where:

- Q is the cumulative heat at a certain time t in hours
- $\dot{Q}_{max}$ is the maximum intensity of heat flow rate
- $t_{\dot{Q}max}$ is the time of maximum heat flow
- $\dot{Q}$ min represents the minimum heat release rate
- $t_{\dot{Q}min}$ is the time when $\dot{Q}$ min is achieved and considered representative of the duration and end of the induction period [91].

Each cumulative heat curve was characterised by a dormant period with a very low heat flow evolution, followed by a peak, marking a period of intense chemical activity and finally a decelerating trench. From Fig. 7-b, as well as, Table 5 and Table 6, it can be seen that the end of the induction period was observed after 2.85 h and 3.60 h ($t_{\dot{Q}min}$) for UHPC and REF paste samples, correspondingly. In addition, the heat flow peak of UHPC and REF were 2.98 and 5.96 kW/kg of cement, respectively, and the time to reach the maximum reaction rate was 8.52 h and 10.33 h, correspondingly.

The shape of calorimetric curves is closely related to the composition of the cementitious matrix [92]. Clinker Portland and pozzolan follow different reaction processes and react at different rates. The rate of pozzolanic reaction depends on the properties of the pozzolan and the mix, as well as, on the temperatures. Previous research has revealed that silica fume can accelerate early-age cement reactions by nucleation and growth site effect [93–95] since it has BET specific surface higher than other pozzolans, the reaction starts earlier [94]. This effect, however, is more prominent as higher the w/c ratio [96]. Shi et al. found that the hydration heat rate of the UHPC was greatly influenced by adding nano-silica (NS) particles. The induction period was drastically reduced by incorporating the NS from 9 h for UHPC without NS to 2.5 h for UHPC-NS samples [97]. Li et al [95] found that the increase of NS addition from 0 to 4 % in UHPC pastes reduced the time to reach the peak from about 40 h to 20 h. The results obtained seemed to be in accordance with previous findings. Nano-sized silica fume particles seem to accelerate the reaction compared with REF mixture (without silica).

In addition, the graphs of Fig. 7 show that at first ages (until 8 h), UHPC presents a higher heating rate than the reference mixture (REF). After the peak is reached, the slope observed in the cumulative heat curve (Fig. 7-b) means that ECat or silica fume is still in progress after the peak. Besides, cumulative heat at 72 h is lower in UHPC than REF mixture. This might be explained by the ECat particles water retention capacity, which can release the absorbed water inside UHPC for longer than 3 days [98]. In addition, the w/c corresponds to 0.21 and 0.23 on REF and UHPC paste samples, and it seems that at 72 h, water was already consumed.

4.3. Autogenous shrinkage

Autogenous shrinkage linear length deformation up 168 h (7 days) is presented in Fig. 8. Deformations ranged between 600 and 1000 μm/m, and the pattern increase shows a similar trend in all mixture compositions under study. Autogenous shrinkage revealed a substantial increase, particularly in the first six hours, afterwards a dramatic reduction in the slope of the curves occurred. Since in UHPC the initial capillary network and the one created by chemical contraction are much finer than the

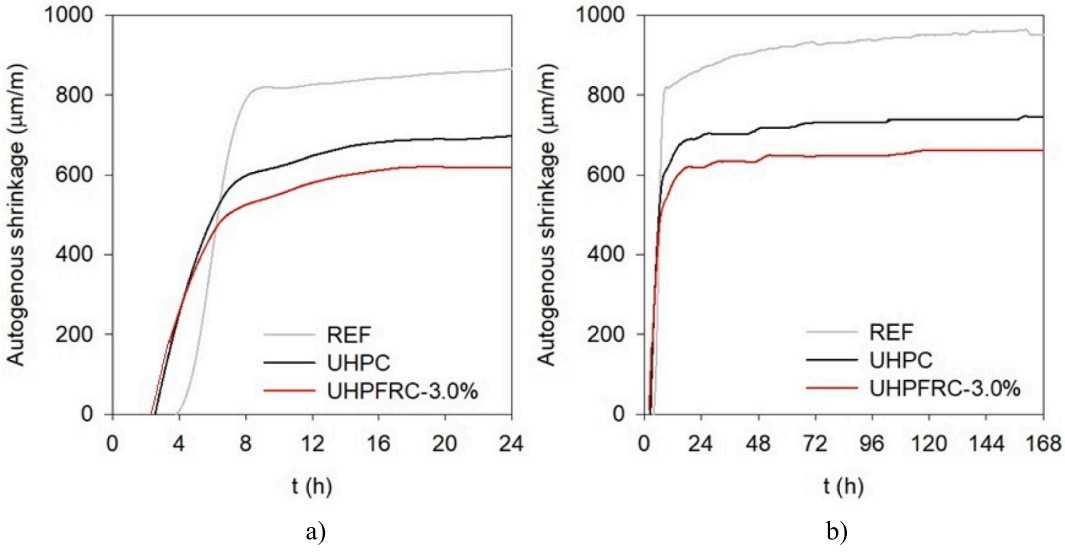

Fig. 8. Autogenous shrinkage evolution: a) up to 24 h; up to 168 h).

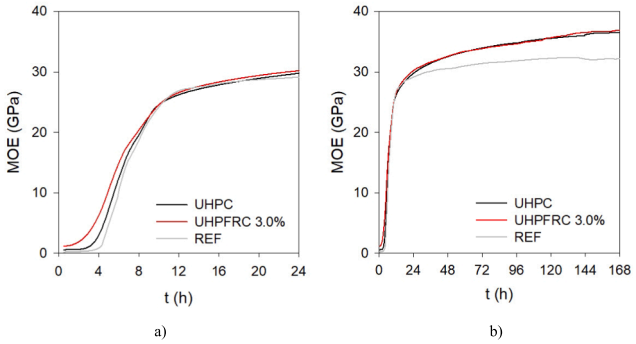

Fig. 9. MOE evolution since casting: a) up to 24 h; up to 168 h).

capillary network of conventional concrete (as C25/30, mostly applied in Portuguese construction), it means that the volumetric contraction due to autogenous shrinkage occurs earlier and increases very rapidly [99].

Wang et al. [100] reported similar trends, in which the autogenous shrinkage of a UHPC (binder: cement + SF + FA) strongly increases in the very first hours and then almost keeps stable after 24 h, reaching 1175 μm/m at 7 days. Ye et al [101] stated that UHPC, including only cement as a binder, achieved approximately 2000 μm/m at 7 days, with a fast rate evolution in the first hours. Meng [91] obtained 1330 μm/m for a UHPC including cement + silica as a binder, while GGBS and FA incorporation reduced autogenous shrinkage to 252–602 μm/m, depending on the dosage incorporation ratio. Nevertheless, it must be stressed that the results of autogenous shrinkage depend "time–zero" definition criterion [87].

Compared to the reference mixture (REF), it is clear that adding 15 % of ECat in UHPC/UHPFRC-3 % reduces autogenous shrinkage effectively. At 24 h a reduction from 800 to 600 μm/m was observed, which means less 25 % of shrinkage. As previously stated [63], ECat was employed as a mitigation strategy against autogenous shrinkage, with additional cost and ecological benefits. Therefore, ECat particles are believed to act as a water reservoir to absorb water during the mixing process. The water retained in ECat particles is then released to restrain the decrease of internal RH caused by cement hydration from a very early age.

The measured shrinkage also depends on the compressibility of the UHPC, particularly their bulk modulus [102]. The stiffness of the cement matrix represents the resistance ability to shrinkage [103]. Even though siliceous sand being replaced by ECat (15 % in volume), the stiffness of the UHPC with ECat, did not decrease; actually, it even slightly improved, as will be presented in Section 4.5. A higher stiffness results in lower deformations at the same driving force. As expected, fibres reduced autogenous shrinkage (UHPC and UHPFRC-3 %).

It must be pointed out that tensile creep at early ages, which has not been investigated in the present study, will also influence autogenous shrinkage.

4.4. MOE evolution since casting

EMM-ARM method identified a wide range of resonant frequencies, from ~ 60 Hz to 200 Hz, within the testing period for the mixture compositions under study. Fig. 9 presents the MOE evolution curves for all tested mixtures up to 168 h (7 days), including a zoom in the first 24 h (Fig. 9-a). As mentioned, each curve is the average result of six tests performed for each mixture, REF, UHPC and UHPFRC-3 %. The MOE evolvement is in accordance with cementitious evolution hydration patterns, in which typically an initial dormant period occurs, roughly between 2 and 4 h in studied mixtures, then a rapid evolution up to 9 h and then keeps evolving with a much lower rate. The dormant period is higher in REF mixture, which corroborates previous results of final setting time (section 4.1), heat of hydration (section 4.2) and autogenous shrinkage (section 4.3).

Table 7
Main MOE values over the time for REF, UHPC and UHPFRC-3%.

Age / MOE (GPa)	*REF*	*UHPC*	*UHPFRC-3 %*
6 h	13.30	14.70	16.47
9 h	23.10	23.81	23.88
1d	29.20	29.80	30.20
2d	30.50	32.60	32.60
7d	32.30	36.60	36.90
14d			37.90
28d			39.20

After 9 h, MOE of REF mixture kept almost constant, while the new UHPC mixture still presented some evolution, which is related to pozzolanic reactions and it is in accordance with previous properties assessed. Previous studies [71] revealed that MOE of UHPC/UHPFRC families increases after 3 days is very small. At 7 days, MOE values of 32.3, 36.6 and 36.9 GPa were achieved for REF, UHPC and UHPFRC-3 %, respectively. UHPFRC-3 % test was extended up to 28 days, reaching 39.2 GPa. Detailed values of MOE are presented in Table 7. As expected, the addition of fibres did not significantly influence MOE, which corroborates with other studies [20,82,70,104].

Yoo et al. [105] obtained a similar MOE evolution pattern after casting using UPV technique. An S-shaped curve elastic modulus development was observed, with a dormant period up to 12 h, followed by a strong evolution up to 24 h, resulting in elastic modulus of 44 GPa at 28 old days. Alsalman et al. [65] measured MOE in the range of 37 to 46 GPa for UHPC mixtures prepared with locally available materials and different contents of steel fibres, which seems to agree with the present study. Sobuz et al. [106] addressed the potential of producing UHPC using widely available fine and coarse aggregates and without the requirement for complex mixing or curing regimes. Four available local aggregates were studied in UHPC mixtures with a target compressive strength in the range 130–160 MPa. The authors achieved MOE between 30 and 38 MPa, depending on aggregate type and proportions. Gesoglu et al. [66] produced low binder UHPC, including NS and/or micro silica (MS), which achieved MOEs between 39 and 42 GPa. Al-Tikrite et al. [72] investigated the MOE experimentally, among others, of Reactive Powder Concrete (RPC) and obtained values between 37 and 44 GPa depending on fibre type and dosage incorporation. A detailed compilation of MOE concerning UHPC/UHPFRC is available in Appendix A.

The MOE of the commercially available UHPC premixes are in the range of 55 to 59 GPa at a reference age of 28 days [5]. Typically, UHPC premixes consist of fine quartz powder (average particle size = 1.7 μm), ultra-fine sand (average particle size = 0.80 mm), and high dosages of cement and silica fume. Those factors provide a denser matrix with a minimum void ratio than the non-proprietary UHPC mixtures, using local materials [5]. This effect is particularly evident in the compressive strength and MOE [65].

4.5. Comparison between hydration kinetics, autogenous shrinkage and young modulus for new UHPC

A comparative analysis of all methods employed to characterise the hardening of UHPC (MOE, autogenous shrinkage, and isothermal calorimetry on UHPC pastes) follows here. Previous research works pointed out that the final setting time of paste (*tf*) is closest to the inflection point of the cumulative heat of the hydration flow curve (Fig. 7-b) in the accelerating stage [107]. However, more recently, Li et al. [95] stated that a difference between *tf* and $t_{\dot{Q}max}$ clearly exists in UHPC paste mixture with incorporation of PCE-type superplasticiser. According to Li et al. [95] these differences occur due to the different mechanisms for setting and hydration kinetics of pastes.

Nevertheless, the end of the accelerating period was determined by

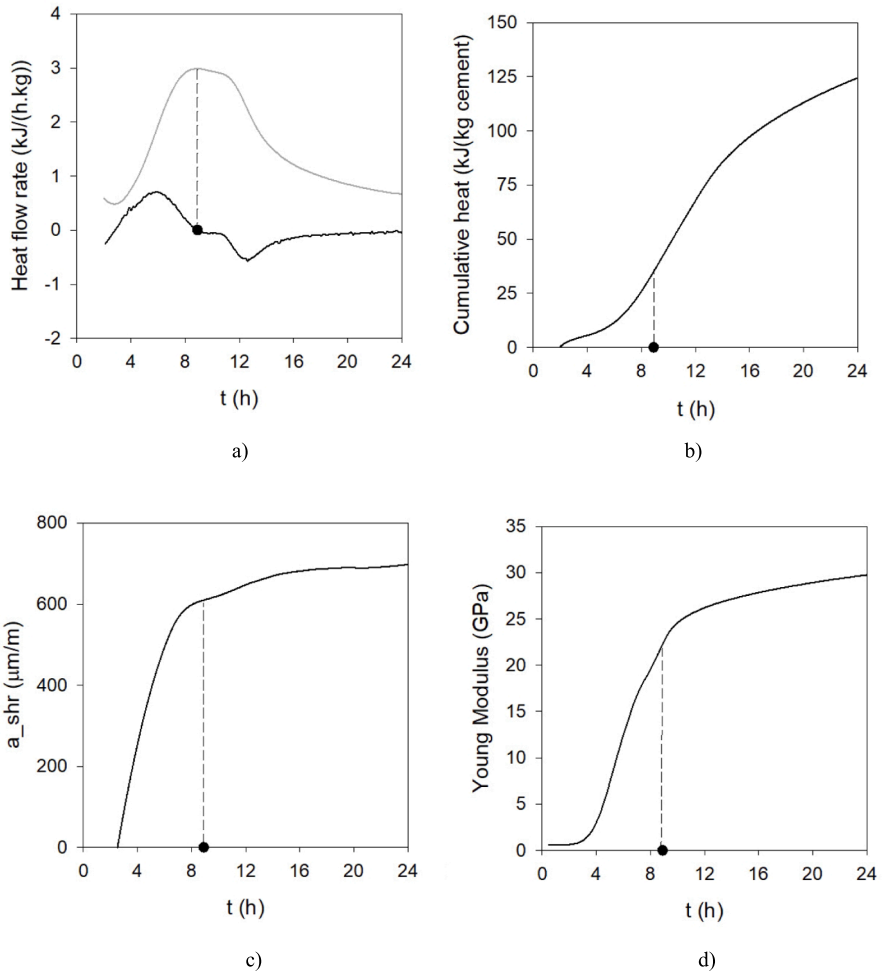

Fig. 10. UHPC aging properties evolution up to 24 h of: a) rate of heat flow (grey) and second derivate of cumulative heat (black); b) cumulative heat of hydration; c) autogenous shrinkage; d) MOE.

the maximum heat rate value, which denotes the beginning of the decelerating period. This point was named the inflection point. The first derivative of the heat flow rate curve, $\ddot{Q}(t)$, can be computed as follows:

$$\ddot{Q}(t) = \frac{\delta \dot{Q}(t)}{\delta t} \tag{1}$$

where $\dot{Q}(t)$ is the heat flow rate (kJ/h) and t is the time (h). This curve can be interpreted as the energy acceleration curve, also observed by Schmidt [107]. Thus, based on the first derivative of the heat flow rate, the inflection point can be calculated as $\ddot{Q}(t) = \frac{\delta \dot{Q}(t)}{\delta t} = 0$.

Fig. 10 presents an integrated overview of early age properties evolution up to 24 h, including the inflexion point corresponding to the black circles in each graph. Fig. 10-a) presents the rate of heat flow (grey line) and the second derivate of cumulative heat calculated according to Equation (1) (black line) for UHPC mixture. In addition, Fig. 10-b) depicts the cumulative heat of hydration, Fig. 10-c) shows the autogenous shrinkage deformation and Fig. 10-d) corresponds to MOE evolution since casting. As can be seen in Fig. 10-b, as well as in Table 5, the inflection point occurs, on average, at 8.52 h. At that time, a great part of young modulus was established, namely, 23.99 GPa (65.5 % considering MOE of 36.60 GPa at 7 days), as well as, most autogenous shrinkage had already occurred, 629 μm/m (84.4 % considering autogenous shrinkage of 745 μm/m at 7 days), see Fig. 10-d. The comparison of different methodologies showed similar kinetics during all test periods, in which at least three stages could be identified. A first dormant stage, where specimens behave closer to a fluid, up to ~ 3 h. Then, when a solid structure starts to form and more hydration products are available, MOE, autogenous shrinkage and heat of hydration start to increase rapidly. Finally, a lower-rate increase stage starts when a high hydration degree is already reached, and further hydration becomes minimal.

5. Conclusions

UHPC/UHPFRC families are advanced materials that seem incompatible with conventional MOE destructive tests, which usually can be performed at the earliest age of 24 h. The current work aimed to improve the understanding of aging characterists of non-proprietary UHPC/UHPFRC-3 % developed by the authors. Comparison between MOE, autogeneous deformation, and heat of hydration were presented. As perceived from the current study, UHPC/UHPFRC-3 % MOE evolution mainly occurred at very early ages, between 3 h and 9 h, which corresponds to the accelerating period. Accelerating period ended about 9 h after cement and water contact, which was determined by the maximum heat rate value from heat of hydration test. In addition, majority of autogenous shrinkage already occurred after approximately 9 h.

EMM-ARM seems to be a promising methodology for assessing the MOE evolution of UHPFRC since casting and has advantages such as the automatic and continuous assessment of MOE. In addition, it can be a powerful tool for general structural numerical modelling and a real-time active quality control measure in production centres. Besides, using NDT methods for evaluating stiffness-related properties from very early age of UHPC/UHPFRC is of utmost importance to take advantage of the

remarkable properties of such advanced material with no waste of time and resources.

CRediT authorship contribution statement

Ana Mafalda Matos: Conceptualization, Methodology, Investigation, Funding acquisition, Data curation, Formal analysis, Visualization, Writing – original draft, Writing – review & editing. **José Granja:** Writing – review & editing. **Sandra Nunes:** Visualization, Supervision, Funding acquisition, Project administration, Writing – review & editing. **José L. Barroso-Aguiar:** Supervision, Funding acquisition, Project administration, Writing – review & editing. **Miguel Azenha:** Writing – review & editing.

Declaration of Competing Interest

The authors declare that they have no known competing financial interests or personal relationships that could have appeared to influence the work reported in this paper.

Data availability

No data was used for the research described in the article.

Acknowledgments

This work was financially supported by: Base Funding—UIDB/04708/2020 and Programmatic Funding—UIDP/04708/2020 of the CONSTRUCT—Instituto de I&D em Estruturas e Construções—funded by national funds through the FCT/MCTES (PIDDAC) and UIDB / 04029/2020 - Institute for Sustainability and Innovation in Structural Engineering (ISISE); by FCT - Fundação para a Ciência e a Tecnologia - through through the individual Scientific Employment Stimulus 2021.01765.CEECIND; and by the project POCI-01-0145-FEDER-031777 – "UHPGRADE - Next generation of ultra-high performance fibre-reinforced cement based composites for rehabilitation and strengthening of the existing infrastructure" funded by FEDER funds through COMPETE2020 - Programa Operacional Competitividade e Internacionalização (POCI) and by national funds (PIDDAC) through FCT/MCTES. Collaboration and materials supply by Sines Refinery/Galp Energia, Secil, Omya Comital, Sika, Bekaert and Chryso Portugal is gratefully acknowledged.

Appendix A

Appendix A
MOE of UHPC/UHPFRC reported in the literature.

Author	*Binder*	*Aggregate*	*w/c*	*Steel Fibre dosage (% or kg/m³)*	*Curing regime*	*fc,28d (MPa)*	*MOE,28d (GPa)*	*MOE methodology assessment*
Current study	Portland Cement + Silica Fume + Limestone filler	Fine silicious sand + ECat	0.23	3 %	Room temperature (20 °C ± 2 °C)	146	39.2	EMM-ARM
Washer et al. [108]	Portland Cement + Silica Fume	Fine Sand	0.19	160 kg/m³	steam cured 90∘C and HR 95 % humidity 48 h		57.27 58.17	ASTM C597 Ultrasonic pulses
							54.96 55.02	ASTM C597 Ultrasonic pulses
Alsalman et al. [65]	CEM I + 20 % condensed silica fume	River sand D_{90} = 1 mm	0.20 (w/b)	0 2 4 6	heat-cured RH 100 % 5 days + 2 days 60 °C + 3 days 90 °C	136.4 137.9 140.8 155.3	43.4 44.5 45.9 45.9	ASTM C 469
	CEM I + 20 % condensed silica fume			0 2 4 6		135.0 135.9 143.2 145.7	37.6 40.3 41.0 43.4	
		Class C fly ash D_{50} = 0.75 mm		0 2 4 6		124.1 128.3 127.6 144.1 135.5 146.8 144.7 162.4	37.2 37.9 40.0 42.7 36.9 38.3 39.3 43.1	
Holschemacher et al [109]	CEM I 42,5 R + Fly ash + Silica-slurry + Silica-fume	Sand 0/2 mm + Quartz sand	0.30			133	49.8	DIN EN 12,390
	CEM I 42,5 R + 0.30 Silica fume	Quartz sand+ Quartz powder	0.25			148	47.1	
	CEM I 42,5 R + 0.18 Silica fume	Sand 0/2 mm + Crushed aggregates 2/5 mm + Quartz sand+ Quartz powder	0.27			144	52.9	
Tue et al. [110]		coarse aggregate < 5 mm				150	56	
Empelmann et al [111]	CEM I 52.5 + Microsilica	Quartz sand 0.125/0.50 mm + Basalt 2/5 + Basalt 5/8	0.24	1.5 1.0 1.25 0.75 2.5	22 days 20 °C and RH 65 % + water curing up to 28 days	144.6 140.8 148.8 146.6 160.8	50.5 51.7 50.2 48.5 52.2	
			0.19–0.20		fog room	140–158	30.1–37.3	

(*continued on next page*)

Appendix A (*continued*)

Author	*Binder*	*Aggregate*	*w/c*	*Steel Fibre dosage (% or kg/m³)*	*Curing regime*	*fc,28d (MPa)*	*MOE,28d (GPa)*	*MOE methodology assessment*
Sobuz et al. [106]	sulphate resisting cement + silica fume	washed river sand < 4.75 mm		0.233* (*Regarding cement mass)				
		mined sand < 4.75 mm				136–158	35.6–40.9	
		Manufacturesand < 4.75 mm				138–153	37.3–38.0	
		granulated lead smelter slag < 4.75 mm				128–131	33.6–36.3	
Gesoglu et al [66]	CEM I 42.5 R	Quartz aggregate in three fractions, 0–0.4, 0.6–1.2, and 1.2–2.5 mm			water curing	116	39	ASTM C469
	CEM I 42.5 R + 0.5 % nano silica					117	39.5	
	CEM I 42.5 R + 1.0 % nano silica					121	40.5	
	CEM I 42.5 R + 2.0 % nano silica					122	41.5	
	CEM I 42.5 R + 3.0 % nano silica					119	41	
	CEM I 42.5 R + 10 % silica fume					120	41	
	CEM I 42.5 R + 10 % silica fume + 0.5 % nano silica					125	42	
	CEM I 42.5 R + 10 % silica fume + 1.0 % nano silica					130	43	
	CEM I 42.5 R + 10 % silica fume + 2.0 % nano silica					131	44	
	CEM I 42.5 R + 10 % silica fume + 3.0 % nano silica					128	43.5	
Krahl et al [67]	Type III Portland cement + silica fume	fine sand < 0.42 mm	0.20	1.0	moist chamber 28 days	134.4	39	ASTM C469
				1.5		146.2	40	
				2.0		148.8	40	
				2.5		148.5	41	
				3.0		151.7	42	
				1.0		134.4	46	Ultrasonic tests by direct method *ACI* 228.2R-13
				1.5		146.2	44	
				2.0		148.8	46	
				2.5		148.5	47	
				3.0		151.7	47	
Zhou and Qiao [112]	Type I/II Portland Cement + Silica Fume	Local natural sand < 0.6 mm	0.18	140 kg/m³	lime-saturated water 23.0 ± 2.0 °C		41	Dynamic modulus test
							42	Wave modulus test with smart aggregates
Gesoglu et al [68]	cement type I 52.5 R + silica fume	Quartz aggregate in three fractions, 0–0.4, 0.6–1.2, and 1.2–2.5 mm	0.195 (w/b)	0.25	water curing	138	39	ASTM C469
				0.5		148	40	
				0.75		149	40	
				1.0		150	41	
				1.5		151	41	
				2.0		152	42	
						153	42	
Ahmad et al [69]	Type I cement + Microsilica	fine dune sand < 1.18 mm	0.18	157 kg/m³	14 days moist curing + 14 days air curing	143.0	56	ASTM C469
	Type I cement + 75 %Microsilica + 25 % Natural pozzolan					138.8	53	
	Type I cement + 50 %Microsilica + 50 % Natural pozzolan					138.2	53	
	90 %Type I cement + 10 %Natural pozzolan + Microsilica					140.4	54	
	80 %Type I cement + 10 %Natural pozzolan + Microsilica					132.2	52	
	70 %Type I cement + 10 %Natural pozzolan + Microsilica					136.0	47	

(*continued on next page*)

Appendix A (*continued*)

Author	*Binder*	*Aggregate*	*w/c*	*Steel Fibre dosage (% or kg/m³)*	*Curing regime*	*fc,28d (MPa)*	*MOE,28d (GPa)*	*MOE methodology assessment*
Hassan et al [70]	Cement + silica fume + Ground Granulated Blast Furnace Slag	Silica sand	0.28	2.0	curing tank 90 °C 48 h + laboratory until testing	120 150	42.08 46	BS 1881–121
Hassan et al [71]	CEM I 52.2 N + silica fume + Ground Granulated Blast Furnace Slag	Silica sand D_{50} = 270 μm	0.28	2.0	curing tank at 90 °C for 48 h + laboratory environment until testing	164.3	46 48 51	BS 1881–121 UPV BS EN 12,504 Resonant frequency testing B.S.1881–209
Tikrite et al [72]	Portland Cement + silica fume	fine sand < 600 μm	0.13	0 1 2 3 4	water curing 20° C (Australian Standards AS 1012.8.1)	100.2 111.8 120.4 121.3 134.0	37 40 40 42 44	*ACI* 318–11
Chozas et al [113]	Cement + silica fume + fly ash	quartz filler and aggregates (0/0.2, 0.1/0.3, and 0.2/1 mm)	0.23		20 °C and HR > 96 %	147.2	49.7	EN 12390–3
	Cement + silica fume + fly ash	quartz filler and aggregates (0/0.2, 0.1/0.3, and 0.2/1 mm)	0.27			135.7	49.9	
	Cement + silica fume + fly ash + ground granulated blast furnace slag	quartz powder (0/100 μm)and aggregates (0/600 μm and 0/2 mm)	0.30			135.0	48.3	
Pyo et al [114]	Cement + silica fume	Silica sand	0.22	2.0	water curing 23 °C	171	48.8	resonant frequencies ASTM C 215

References

[1] G. Tilly, Performances of concrete repairs in practice, (n.d.).
[2] A.M. Matos, S. Nunes, C. Costa, J.L.B. Aguiar, Durability of an UHPC containing spent equilibrium catalyst, Constr. Build. Mater. 305 (2021), 124681, https://doi.org/10.1016/J.CONBUILDMAT.2021.124681.
[3] W. Wang, J. Liu, F. Agostini, C.A. Davy, F. Skoczylas, D. Corvez, Durability of an ultra high performance fiber reinforced concrete (UHPFRC) under progressive aging, Cem. Concr. Res. 55 (2014) 1–13, https://doi.org/10.1016/J.CEMCONRES.2013.09.008.
[4] T. Stengel, P. Schießl, Life cycle assessment (LCA) of ultra high performance concrete (UHPC) structures, Eco-Efficient Construction and Building Materials: Life Cycle Assessment (LCA), Eco-Labelling and Case, Studies. (2014) 528–564, https://doi.org/10.1533/9780857097729.3.528.
[5] B.A. Graybeal, H.G. Russel, Ultra-High Performance Concrete: A State-of-the-Art Report for the Bridge Community. Publication N.º FHWA-HRT-13-060, 2013.
[6] E. Brühwiler, E. Denarié, Rehabilitation of concrete structures using Ultra-High Performance Fibre Reinforced Concrete, in: UHPC-2008: The Second International Symposium on Ultra High Performance Concrete, Kassel, Germany, 2008: pp. 1–8.
[7] G. Habert, E. Denarié, A. Šajna, P. Rossi, Lowering the global warming impact of bridge rehabilitations by using Ultra High Performance Fibre Reinforced Concretes, Cem. Concr. Compos. 38 (2013) 1–11, https://doi.org/10.1016/J.CEMCONCOMP.2012.11.008.
[8] B. Graybeal, E. Brühwiler, B.-S. Kim, F. Toutlemonde, Y.L. Voo, A. Zaghi, International perspective on UHPC in bridge engineering, J. Bridg. Eng. 25 (2020) 04020094, https://doi.org/10.1061/(ASCE)BE.1943-5592.0001630.
[9] E. Denarié, UHPFRC for the cast-in place reinforcement of offshore maritime signalisation structures, in: HAC2018 | V Congreso Iberoamericano de Hormigón Autocompactante y Hormigones Especiales, Universitat Politècnica de València, Valencia, 2018. 10.4995/hac2018.2018.8261.
[10] N.M. Azmee, N. Shafiq, Ultra-high performance concrete: From fundamental to applications, Case Stud. Constr. Mater. 9 (2018) e00197.
[11] E. Brühwiler, E. Denarié, Rehabilitation and strengthening of concrete structures using ultra-high performance fibre reinforced concrete, Struct. Eng. Int. 4 (2013) 450–457, https://doi.org/10.2749/101686613X13627347100437.
[12] E. Bruhwiler, E. Denarie, Rehabilitation and strengthening of concrete structures using ultra-high performance fibre reinforced concrete, Struct. Eng. Int. 23 (2013) 450–457, https://doi.org/10.2749/101686613X13627347100437.
[13] S. Nabaei, S. Nendaz, Rehabilitation of transportation infrastructures: the potential of new materials, in: IABSE Conference – Structural Engineering: Providing Solutions to Global Challenges, Geneva, Switzerland, 2015.
[14] K. Zmetra, A.E. Zaghi, K. Wille, Rehabilitation of Steel Bridge Girders with Corroded Ends Using Ultra-High Performance Concrete, Structures Congress 2015 - Proceedings of the 2015 Structures Congress. (2015) 1411–1422. 10.1061/9780784479117.121.
[15] B.A. Tayeh, B.H.A. Bakar, M.A.M. Johari, Y.L. Voo, Utilisation of ultra-high performance fibre concrete (UHPFC) for rehabilitation – A REVIEW, Procedia Eng. 54 (2013) 525–538, https://doi.org/10.1016/j.proeng.2013.03.048.
[16] Peter Racky, Cost-effectiveness and sustainability of UHPC, in: International Symposium on Ultra High Performance Concrete, Kassel, Germany, 2004: pp. 797–805.
[17] N. Randl, T. Steiner, S. Ofner, E. Baumgartner, T. Mészöly, Development of UHPC mixtures from an ecological point of view, Constr. Build. Mater. 67 (2014) 373–378, https://doi.org/10.1016/j.conbuildmat.2013.12.102.
[18] AFGC, Documents scientifiques et techniques Bétons fibrés à ultra-hautes performances - recommandations, (2013) 358.
[19] S. Abbas, M.L. Nehdi, M.A. Saleem, Ultra-high performance concrete: mechanical performance, durability, sustainability and implementation challenges, Int. J. Concr. Struct. Mater. 10 (2016) 271–295, https://doi.org/10.1007/s40069-016-0157-4.
[20] K. Habel, Structural behaviour of elements combining Ultra-High Performance Fibre Reinforced Concretes (UHPFRC) and Reinforced Concrete, École Polytechnique Fédérale de Lausanne (2004), https://doi.org/10.5075/epfl-thesis-3036.
[21] K. Habel, J. Charron, E. Denarie, E. Bruehwiler, Autogenous deformations and viscoelasticity of UHPFRC in structures. Part I: experimental results, Mag. Concr. Res. 58 (2006).
[22] A. Switek-Rey, E. Denarié, E. Brühwiler, Early age creep and relaxation of UHPFRC under low to high tensile stresses, Cem. Concr. Res. 83 (2016) 57–69, https://doi.org/10.1016/j.cemconres.2016.01.005.
[23] I. Schachinger, K. Schmidt, D. Heinz, P. Schießl, Early-Age Cracking Risk and Relaxation by Restrained Autogenous Deformation of Ultra High Performance Concrete, in: 6th Internacional Symposio of High Strength/High Performance Concrete, Leipzig, 2002: pp. 1341–1354.
[24] M. Kazemi Kamyab, Autogenous Shrinkage and Hydration Kinetics of SH-UHPFRC under Moderate to Low Temperature Curing Conditions, Ecole Polytechnique Fédérale de Lausanne, Switzerland , 2013. 10.5075/EPFL-THESIS-5681.
[25] D.-Y. Yoo, K.-H. Min, J.-H. Lee, Y.-S. Yoon, Shrinkage and cracking of restrained ultra-high-performance fiber-reinforced concrete slabs at early age, Constr. Build. Mater. 73 (2014) 357–365, https://doi.org/10.1016/j.conbuildmat.2014.09.097.
[26] D. Wang, C. Shi, Z. Wu, J. Xiao, Z. Huang, Z. Fang, A review on ultra high performance concrete: Part II. Hydration, microstructure and properties, (n.d.). 10.1016/j.conbuildmat.2015.08.095.
[27] O.M. Abdulkareem, A. Ben Fraj, M. Bouasker, A. Khelidj, Mixture design and early age investigations of more sustainable UHPC, Constr. Build. Mater. 163 (2018) 235–246, https://doi.org/10.1016/J.CONBUILDMAT.2017.12.107.
[28] E.C. Torregrosa, Dosage Optimisation and Bolted Connections for UHPFRC ties, Universitat Politècnica de València, 2013.
[29] L. Sorelli, R. Davila, F.-J. Ulm, V. Perry, P. Seibert, Risk Analysis of Early-Age Cracking in UHPC Structures, in: Second International Symposium on Ultra-High Performance Concrete, Kassel, Germany, 2008: pp. 331–338.

[30] ASTM C469/C469M - 14 Standard Test Method for Static Modulus of Elasticity and Poisson's Ratio of Concrete in Compression, (2014).
[31] ISO 1920-10:2010. Testing of concrete - Part 10: Determination of static modulus of elasticity in compression, (2010).
[32] M. Azenha, R. Faria, F. Magalhaes, L. Ramos, A. Cunha, Measurement of the E-modulus of cement pastes and mortars since casting, using a vibration based technique, Mater. Struct. 45 (2012) 81–92, https://doi.org/10.1617/s11527-011-9750-9.
[33] C. Boulay, E. Merliot, S. Staquet, O. Marzouk, Monitoring of the concrete setting with an automatic method, in: 13th International Conference and Exhibition : Structural Faults and Repair, 2010.
[34] C. Boulay, S. Staquet, B. Delsaute, J. Carette, M. Crespini, O. Yazoghli-Marzouk, Rick Merliot, S. Ramanich, How to monitor the modulus of elasticity of concrete, automatically since the earliest age? Mater. Struct. 47 (2014) 141–155, https://doi.org/10.1617/s11527-013-0051-3.
[35] S. Staquet, B. Delsaute, A. Darquennes, B. Espion, Testing concrete since setting time under free and restraint conditions with a revisited TSTM, CONCRACK 3 – RILEM-JCI International Workshop on Crack Control of Mass Concrete and Related Issues Concerning Early-Age of Concrete Structures, 15-16 March 2012, Paris, France. (2012) 12.
[36] J. Silva, M. Azenha, G. Correia, C. Ferreira, Continuous stiffness assessment of cement-stabilised soils from early age, Géotechnique. 63 (2013) 1419–1432, https://doi.org/10.1680/geot.13.P.021.
[37] J.H. Kim, S.P. Shah, Z. Sun, H.-G. Kwak, Ultrasonic wave reflection and resonant frequency measurements for monitoring early-age concrete, J. Mater. Civ. Eng. 21 (2009) 476–483, https://doi.org/10.1061/(ASCE)0899-1561(2009)21:9(476).
[38] V.M. Malhotra, N.J. Carino, Handbook on non-destructive testing of concrete, 2004.
[39] D.S. Wang, L.P. Yu, H.P. Zhu, Strength monitoring of concrete based on embedded PZT transducer and the resonant frequency, in: Proceedings of the 2010 Symposium on Piezoelectricity, Acoustic Waves and Device Applications, SPAWDA10, IEEE, Xiamen, China, 2010: pp. 202–205. 10.1109/SPAWDA.2010.5744303.
[40] M. Azenha, F. Magalhães, R. Faria, Á. Cunha, Measurement of concrete E-modulus evolution since casting: A novel method based on ambient vibration, Cem. Concr. Res. 40 (2010) 1096–1105, https://doi.org/10.1016/j.cemconres.2010.02.014.
[41] J. Granja, M. Azenha, Continuous monitoring of concrete mechanical properties since early age to support construction phasing, in: CONCREEP-10 Mechanics and Physics of Creep, Shrinkage, and Durability of Concrete and Concrete Structures, 2015. 10.1061/9780784479346.161.
[42] B. Delsaute, C. Boulay, J. Granja, J. Carette, M. Azenha, C. Dumoulin, G. Karaiskos, A. Deraemaeker, S. Staquet, Testing Concrete E-modulus at Very Early Ages Through Several Techniques: An Inter-laboratory Comparison, Strain. (2016) 91–109. 10.1111/str.12172.
[43] M. Azenha, L.F. Ramos, R. Aguilar, J.L. Granja, Continuous monitoring of concrete E-modulus since casting based on modal identification: A case study for in situ application, Cem. Concr. Compos. 34 (2012) 881–890, https://doi.org/10.1016/j.cemconcomp.2012.04.004.
[44] L. Maia, M. Azenha, R. Faria, J. Figueiras, Influence of the cementitious paste composition on the E-modulus and heat of hydration evolutions, Cem. Concr. Res. 41 (2011) 799–807, https://doi.org/10.1016/J.CEMCONRES.2011.03.008.
[45] L. Maia, M. Azenha, M. Geiker, J. Figueiras, E-modulus evolution and its relation to solids formation of pastes from commercial cements, Cem. Concr. Res. 42 (2012) 928–936, https://doi.org/10.1016/j.cemconres.2012.03.013.
[46] L. Maia, M. Azenha, R. Faria, J. Figueiras, Identification of the percolation threshold in cementitious pastes by monitoring the E-modulus evolution, Cem. Concr. Compos. 34 (2012) 739–745, https://doi.org/10.1016/j.cemconcomp.2012.03.001.
[47] J.L. Granja, M. Azenha, C. De Sousa, C. Ferreira, T. Matsuda, H. Kawakami, T. Koide, T. Noguchi, Comparison between different experimental techniques for stiffness monitoring of cement pastes, J. Adv. Concr. Technol. 12 (2014) 261–271, https://doi.org/10.3151/jact.12.47.
[48] J. Granja, M. Azenha, Towards a robust and versatile method for monitoring E-modulus of concrete since casting: enhancements and extensions of EMM-ARM, Strain 53 (2017) e12232.
[49] J.L.D. Granja, Continuous Characterisation of Stiffness of Cement based Materials: Experimental Analysis and Micro-Mechanics Modelling, University of Minho, 2016.
[50] R. Yu, P. Spiesz, H.J.H. Brouwers, Development of an eco-friendly Ultra-High Performance Concrete (UHPC) with efficient cement and mineral admixtures uses, Cem. Concr. Compos. 55 (2015) 383–394, https://doi.org/10.1016/J.CEMCONCOMP.2014.09.024.
[51] X. Wang, R. Yu, Z. Shui, Z. Zhao, Q. Song, B. Yang, D. Fan, Development of a novel cleaner construction product: Ultra-high performance concrete incorporating lead-zinc tailings, J. Clean. Prod. 196 (2018) 172–182, https://doi.org/10.1016/J.JCLEPRO.2018.06.058.
[52] X. Wang, R. Yu, Z. Shui, Q. Song, Z. Liu, M. Bao, Z. Liu, S. Wu, Optimised treatment of recycled construction and demolition waste in developing sustainable ultra-high performance concrete, J. Clean. Prod. 221 (2019) 805–816, https://doi.org/10.1016/J.JCLEPRO.2019.02.201.
[53] M. Amin, B.A. Tayeh, M.A. Kandil, I.S. Agwa, M.F. Abdelmagied, Effect of rice straw ash and palm leaf ash on the properties of ultrahigh-performance concrete, Case Stud. Constr. Mater. 17 (2022) e01266.
[54] Y. Lv, L. Yang, J. Wang, B. Zhan, Z. Xi, Y. Qin, D. Liao, Performance of ultra-high-performance concrete incorporating municipal solid waste incineration fly ash, Case Stud. Constr. Mater. 17 (2022) e01155.
[55] A. Rajasekar, K. Arunachalam, M. Kottaisamy, V. Saraswathy, Durability characteristics of Ultra High Strength Concrete with treated sugarcane bagasse ash, Constr. Build. Mater. 171 (2018) 350–356, https://doi.org/10.1016/J.CONBUILDMAT.2018.03.140.
[56] P.P. Li, Q.L. Yu, H.J.H. Brouwers, Effect of coarse basalt aggregates on the properties of Ultra-high Performance Concrete (UHPC), Constr. Build. Mater. 170 (2018) 649–659, https://doi.org/10.1016/J.CONBUILDMAT.2018.03.109.
[57] A. Arora, Y. Yao, B. Mobasher, N. Neithalath, Fundamental insights into the compressive and flexural response of binder- and aggregate-optimised ultra-high performance concrete (UHPC), Cem. Concr. Compos. 98 (2019) 1–13, https://doi.org/10.1016/J.CEMCONCOMP.2019.01.015.
[58] Z. Yu, L. Wu, Z. Yuan, C. Zhang, T. Bangi, Mechanical properties, durability and application of ultra-high-performance concrete containing coarse aggregate (UHPC-CA): A review, Constr. Build. Mater. 334 (2022), https://doi.org/10.1016/J.CONBUILDMAT.2022.127360.
[59] A.M. Matos, Design of eco-efficient ultra-high performance fibre reinforced cement-based composite for rehabilitation/strengthening applications, 2020. https://sigarra.up.pt/reitoria/en/pub_geral.pub_view?pi_pub_base_id=381627 (accessed December 26, 2021).
[60] A.M. Matos, S. Nunes, J.L. Barroso Aguiar, Capillary transport of water in cracked and non-cracked UHPFRC specimens, J. Adv. Concr. Technol. 17 (2019) 244–259, https://doi.org/10.3151/JACT.17.244.
[61] A.M. Matos, S. Chaves-Figueiredo, S. Nunes, E. Schlangen, Durability of an UHPFRC under mechanical and chloride loads, Constr. Build. Mater. 311 (2021), https://doi.org/10.1016/j.conbuildmat.2021.125223.
[62] A.M. Matos, S. Nunes, C. Costa, J.L. Barroso-Aguiar, Characterisation of Non-proprietary UHPC for Use in Rehabilitation/Strengthening Applications, in: Mechtcherine V., Khayat K., Secrieru E. (Eds.), RILEM Bookseries. International Conference on Rheology and Processing of Construction Materials International Symposium on Self-Compacting Concrete, Springer, Cham, 2019: pp. 552–559. 10.1007/978-3-030-22566-7_64.
[63] A.M. Matos, S. Nunes, C. Costa, J.L. Barroso-Aguiar, Spent equilibrium catalyst as internal curing agent in UHPFRC, Cem. Concr. Compos. 104 (2019), https://doi.org/10.1016/J.CEMCONCOMP.2019.103362.
[64] A.M. Matos, S. Nunes, S. Chaves Figueiredo, E. Schlangen, J.L.B. Aguiar, A.M. Matos, Á.S. Nunes, S.C. Figueiredo, Á.E. Schlangen, J.L.B. Aguiar, Chloride Ion Penetration into Cracked UHPFRC During Wetting-drying Cycles, in: Valente I.B., Ventura Gouveia A., Dias S.S (Eds.), RILEM Bookseries. Proceedings of the 3rd RILEM Spring Convention and Conference (RSCC 2020), Springer, Cham, 2020: pp. 227–238. 10.1007/978-3-030-76551-4_21.
[65] A. Alsalman, C.N. Dang, G.S. Prinz, W.M. Hale, Evaluation of modulus of elasticity of ultra-high performance concrete, Constr. Build. Mater. 153 (2017) 918–928, https://doi.org/10.1016/J.CONBUILDMAT.2017.07.158.
[66] M. Gesoglu, E. Güneyisi, D.S. Asaad, G.F. Muhyaddin, Properties of low binder ultra-high performance cementitious composites: Comparison of nanosilica and microsilica, Constr. Build. Mater. 102 (2016) 706–713, https://doi.org/10.1016/J.CONBUILDMAT.2015.11.020.
[67] P.A. Krahl, G. de Miranda Saleme, R.C. Gidrão, Compressive behavior of UHPFRC under quasi-static and seismic strain rates considering the effect of fiber content, Constr. Build. Mater. 188 (2018) 633–644, https://doi.org/10.1016/J.CONBUILDMAT.2018.08.121.
[68] M. Gesoglu, E. Güneyisi, G.F. Muhyaddin, D.S. Asaad, Strain hardening ultra-high performance fiber reinforced cementitious composites: Effect of fiber type and concentration, Compos. B Eng. 103 (2016) 74–83, https://doi.org/10.1016/J.COMPOSITESB.2016.08.004.
[69] S. Ahmad, K.O. Mohaisen, S.K. Adekunle, S.U. Al-Dulaijan, M. Maslehuddin, Influence of admixing natural pozzolan as partial replacement of cement and microsilica in UHPC mixtures, Constr. Build. Mater. 198 (2019) 437–444, https://doi.org/10.1016/J.CONBUILDMAT.2018.11.260.
[70] A.M.T. Hassan, S.W. Jones, G.H. Mahmud, Experimental test methods to determine the uniaxial tensile and compressive behaviour of ultra high performance fibre reinforced concrete (UHPFRC), Constr. Build. Mater. 37 (2012) 874–882, https://doi.org/10.1016/J.CONBUILDMAT.2012.04.030.
[71] A.M.T. Hassan, S.W. Jones, Non-destructive testing of ultra high performance fibre reinforced concrete (UHPFRC): A feasibility study for using ultrasonic and resonant frequency testing techniques, Constr. Build. Mater. 35 (2012) 361–367, https://doi.org/10.1016/j.conbuildmat.2012.04.047.
[72] A. Al-Tikrite, M.N.S. Hadi, Mechanical properties of reactive powder concrete containing industrial and waste steel fibres at different ratios under compression, Constr. Build. Mater. 154 (2017) 1024–1034, https://doi.org/10.1016/J.CONBUILDMAT.2017.08.024.
[73] O. Tsioulou, A. Lampropoulos, S. Paschalis, Combined Non-Destructive Testing (NDT) method for the evaluation of the mechanical characteristics of Ultra High Performance Fibre Reinforced Concrete (UHPFRC), Constr. Build. Mater. 131 (2017) 66–77, https://doi.org/10.1016/j.conbuildmat.2016.11.068.
[74] B.A. Graybeal, Characterisation of the Behavior of Ultra-high Performance Concrete, University of Maryland, 2005.
[75] A.M. Matos, S. Nunes, C. Costa, J.L. Barroso-Aguiar, Characterisation of Non-proprietary UHPC for Use in Rehabilitation/Strengthening Applications, in: V. Mechtcherine, K. Khayat, E. Secrieru (Eds.), RILEM Bookseries, Springer Netherlands, 2020: pp. 552–559. 10.1007/978-3-030-22566-7_64.

[76] A.M. Matos, Susceptibility to Expansive Reactions of a Greener UHPC: Micro to Macro-Scale Study, Applied Sciences 2022, Vol. 12, Page 6252. 12 (2022) 6252. 10.3390/APP12126252.

[77] Wexham Developments, JAF Calorimeter - Operating Manual, Edition 7, United Kingdoom, 2005.

[78] Kay Wille, A.E. Naaman, G.J. Parra-Montesinos, Ultra-High Performance Concrete with Compressive Strength Exceeding 150 MPa (22 ksi): A Simpler Way, ACI Mater J. 108 (2011). 10.14359/51664215.

[79] W. Meng, M. Valipour, K.H. Khayat, Optimisation and performance of cost-effective ultra-high performance concrete, Mater. Struct. 50 (2017) 29, https://doi.org/10.1617/s11527-016-0896-3.

[80] E. Brühwiler, "Structural UHPFRC": Welcome to the post-concrete era!, in: First International Interactive Symposium on UHPC, Des Moines, Iowa, 2016. 10.21838/uhpc.2016.key.

[81] E. Denarié, Recommendations for the tailoring of UHPFRC recipes for rehabilitation: Deliverable ARCHES D06, (2010).

[82] M.B. Eide, J.-M. Hisda, L, Ultra High Performance Fibre Reinforced Concrete (UHPFRC) – State of the art. COIN Project report 44-2012, Oslo, 2012.

[83] D. Wang, C. Shi, Z. Wu, J. Xiao, Z. Huang, Z. Fang, A review on ultra high performance concrete: Part II. Hydration, microstructure and properties, Constr Build Mater. 96 (2015) 368–377. 10.1016/j.conbuildmat.2015.08.095.

[84] I. Markovic, High-Performance Hybrid-Fibre Concrete – Development and Utilisation, Delft University, 2006.

[85] K. Wille, A.E. Naaman, S. El-Tawil, G.J. Parra-Montesinos, Ultra-high performance concrete and fiber reinforced concrete: achieving strength and ductility without heat curing, Mater. Struct. 45 (2012) 309–324, https://doi.org/10.1617/s11527-011-9767-0.

[86] Z.B. Haber, I.D. la Varga, B.A. Graybeal, Properties and Behavior of UHPC-Class Materials (FHWA-HRT-18-036), McLean, VA, 2018.

[87] H. Huang, G. Ye, Examining the "time-zero" of autogenous shrinkage in high/ultra-high performance cement pastes, Cem. Concr. Res. 97 (2017) 107–114, https://doi.org/10.1016/j.cemconres.2017.03.010.

[88] A. Allahverdi, S. Vakilinia, P. Gharabeglu, Effects of RFCC spent catalyst on some physiomechanical properties of Portland cement, Ceramics-Silikáty 55 (2011) 161–168.

[89] J. Paya, J. Monzo, M.V. Borrachero, Physical, chemical and mechanical properties of fluid catalytic cracking catalyst residue (FC3R) blended cements, Cem. Concr. Res. 31 (2001) 57–61, https://doi.org/10.1016/S0008-8846(00)00432-4.

[90] N. Su, H.-Y. Fang, Z.-H. Chen, F.-S. Liu, Reuse of waste catalysts from petrochemical industries for cement substitution, Cem. Concr. Res. 30 (2000) 1773–1783, https://doi.org/10.1016/S0008-8846(00)00401-4.

[91] W. Meng, Design and Performance of Cost-Effective Ultra-High Performance Concrete for Prefabricated Elements, University of Science and Technology, Missouri, 2017.

[92] B. Pacewska, I. Wiliñska, M. Bukowska, Calorimetric investigations of the influence of waste aluminosilicate on the hydration of different cements, J. Therm. Anal. Calorim. 97 (2009) 61–66.

[93] J. Zelić, D. Rušić, D. Veža, R. Krstulović, The role of silica fume in the kinetics and mechanisms during the early stage of cement hydration, Cem. Concr. Res. 30 (2000) 1655–1662, https://doi.org/10.1016/S0008-8846(00)00374-4.

[94] P. Hewlett, Lea's Chemistry of Cement and Concrete, 4th ed., Elsevier Science & Technology Books, Amsterdam, 2004. 10.1016/B978-0-7506-6256-7.50031-X.

[95] P.P. Li, Q.L. Yu, H.J.H. Brouwers, Effect of PCE-type superplasticiser on early-age behaviour of ultra-high performance concrete (UHPC), Constr. Build. Mater. 153 (2017) 740–750, https://doi.org/10.1016/J.CONBUILDMAT.2017.07.145.

[96] B.W. Langan, K. Weng, M.A. Ward, Effect of silica fume and fly ash on heat of hydration of Portland cement, Cem. Concr. Res. 32 (2002) 1045–1051, https://doi.org/10.1016/S0008-8846(02)00742-1.

[97] Y. Shi, G. Long, C. Ma, Y. Xie, J. He, Design and preparation of ultra-high performance concrete with low environmental impact, J. Clean. Prod. 214 (2019) 633–643, https://doi.org/10.1016/J.JCLEPRO.2018.12.318.

[98] S.-H. Kang, S.-G. Hong, J. Moon, Importance of drying to control internal curing effects on field casting ultra-high performance concrete, Cem. Concr. Res. 108 (2018) 20–30, https://doi.org/10.1016/J.CEMCONRES.2018.03.008.

[99] P.C. Aïtcin, High Performance Concrete (HPC), 36th Conference on Our World in Concrete & Structures. (2011) 14–16.

[100] X. Wang, R. Yu, Z. Shui, Q. Song, Z. Zhang, Mix design and characteristics evaluation of an eco-friendly Ultra-High Performance Concrete incorporating recycled coral based materials, J. Clean. Prod. 165 (2017) 70–80, https://doi.org/10.1016/j.jclepro.2017.07.096.

[101] G. Ye, N. Van Tuan, H. Huang, Rice Hush Ash as smart material to mitigate autogenous shrinkage in high (ultra-high) performance concrete, in: Third International Conference on Sustainable Construction Materials and Technologies (SCMT2013), At Kyoto, Japan, 2013.

[102] J. Justs, M. Wyrzykowski, D. Bajare, P. Lura, Internal curing by superabsorbent polymers in ultra-high performance concrete, Cem. Concr. Res. 76 (2015) 82–90, https://doi.org/10.1016/j.cemconres.2015.05.005.

[103] H. Huang, G. Ye, Use of rice rusk rsh for ritigating the autogenous rhrinkage of rement rastes at low rater rement ratio, in: HiPerMat 2016: Ultra-High Performance Concrete and High Performance Construction Materials Figure, 2016: pp. 1–9.

[104] O. Bonneau, C. Poulin Jr., M. Dugat, P.-C.-A. Tcin, Reactive powder concretes: from theory to practice, Concr. Int. 18 (1996) 47–49.

[105] D.-Y. Yoo, J.-J. Park, S.-W. Kim, Y.-S. Yoon, Early age setting, shrinkage and tensile characteristics of ultra high performance fiber reinforced concrete, Constr. Build. Mater. 41 (2013) 427–438, https://doi.org/10.1016/J.CONBUILDMAT.2012.12.015.

[106] H.R. Sobuz, P. Visintin, M.S. Mohamed Ali, M. Singh, M.C. Griffith, A.H. Sheikh, Manufacturing ultra-high performance concrete utilising conventional materials and production methods, Constr. Build. Mater. 111 (2016) 251–261, https://doi.org/10.1016/J.CONBUILDMAT.2016.02.102.

[107] W. Schmidt, Design Concepts for the Robustness Improvement of Self-Compacting Concrete : Effects of Admixtures and Mixture Components on the Rheology and Early Hydration at Varying Temperatures, Eindhoven University of Technology Library, 2014, 10.6100/IR771936.

[108] G. Washer, P. Fuchs, B.A. Graybeal, J.L. Hartmann, Ultrasonic testing of reactive powder concrete, IEEE Trans. Ultrason. Ferroelectr. Freq. Control 51 (2004) 193–201, https://doi.org/10.1109/TUFFC.2004.1320767.

[109] K. Holschemacher, D. Weisse, S. Klotz, Bond of Reinforcement in Ultra High Strength Concrete, in: M. Schmidt, E. Fehling, C. Geisenhanslüke (Eds.), Proceedings of the International Symposium on Ultra High Performance Concrete, 2004: pp. 375–387.

[110] N.V. Tue, M. Küchler, Load and deformation behaviour of confined ultra high performance concrete dowels, in: E. Fehling, M. Schmidt, S. Stürwald (Eds.), Second International Symposium on Ultra High Performance Concrete, Kassel, Germany, 2008, pp. 553–554.

[111] M. Empelmann, M. Teutsch, G. Steven, Improvement of the post fracture behaviour of UHPC by fibres, in: E. Fehling, M. Schmidt, S. Stürwald (Eds.), Second International Symposium on Ultra High Performance Concrete, Kassel, Germany, 2008.

[112] Z. Zhou, P. Qiao, Durability of ultra-high performance concrete in tension under cold weather conditions, Cem. Concr. Compos. 94 (2018) 94–106, https://doi.org/10.1016/J.CEMCONCOMP.2018.08.019.

[113] V. Chozas, Larraza, J. Vera-Agullo, N. Williams-Portal, U. Mueller, N. Da Silva, M. Flansbjer, Synthesis and characterisation of reactive powder concrete for its application on thermal insulation panels, IOP Conf Ser Mater Sci Eng. 96 (2015). 10.1088/1757-899X/96/1/012044.

[114] S. Pyo, M. Tafesse, H. Kim, H.-K. Kim, Effect of chloride content on mechanical properties of ultra high performance concrete, Cem. Concr. Compos. 84 (2017) 175–187, https://doi.org/10.1016/J.CEMCONCOMP.2017.09.006.